Plasma Aerodynamic Control Effectors for Improved Wind Turbine Performance

Phase I SBIR Final Report

August 2008

Grant No. DE-FG02-07ER84781
Contract Period: 06/20/2007 - 03/19/2008

Prepared by:

Mehul P. Patel (PI), Srikanth Vasudevan
Robert C. Nelson, Thomas C. Corke

Award Recipient: Orbital Research Inc.
4415 Euclid Ave, STE 500
Cleveland, OH 44103-3733
Phone: (216) 649-0399
Fax: (216) 649-0347

Submitted to:

Dennis Lin, DOE Project Officer
U.S. Department OF Energy
1000 Independence Ave, S.W.
Washington D.C. 20585-1290

Table of Contents

Nomenclature

a	angle of attack
a_s	stall angle of attack
p	density of air
C	airfoil chord length
C_d	drag coefficient
C_f	flap chord length
C_l	lift coefficient
C_r	trailing-edge ramp chord length
$C_{l\,max}$	maximum lift coefficient
f	excitation frequency of unsteady DBD actuator= 1/Tcontrol
L_{sep}	streamwise extent of separation zone, m
q	dynamic pressure
Re_c	Reynolds number based on axial chord length and free-stream velocity
$T_{Control}$	time period for unsteady operation = 1/f
T_{signal}	actuator on time period for unsteady operation
U_∞	free-stream velocity
x,y,z	axial coordinates

FOREWORD

This technical report summarizes the work performed by Orbital Research Inc. (ORI), Cleveland, Ohio, under a Department of Energy (DOE) SBIR Phase I Grant DE-FG02-07ER84781, Plasma Aerodynamic Control Effectors (PACE) for Improved Wind Turbine Performance. The period of performance was from June 2007 to March 2008. Dennis Lin was the DOE Project Monitor for this grant.

ACKNOWLEDGMENTS

The authors wish to acknowledge the support of Dennis Lin of DOE for his encouragement and support during the Phase I effort. The authors also wish to acknowledge Terry Ng and Ed Santavicca of Orbital Research Inc. and Hesham Otham of University of Notre Dame for providing technical support during the wind tunnel experiments.

1. Summary

Rotor blades on current wind turbines are either designed to stall or employ expensive and complex pitch control systems to maintain control under adverse wind conditions such as gusts, varying speeds, etc. The former limits the efficiency of the wind turbine, and the latter leads to high capital costs and non-competitive return on investment. Additionally, the acceptance of wind turbines is hindered due to operational costs associated with repair and maintenance from stress degradation of system components.

Orbital Research Inc. (ORI), in collaboration with the University of Notre Dame (UND), is developing an innovative Plasma Aerodynamic Control Effectors (PACE) technology for improved performance of wind turbines. The PACE system is aimed towards the design of "smart" rotor blades to enhance energy capture and reduce aerodynamic loading and noise using flow-control. The PACE system will provide ability to change aerodynamic loads and pitch distribution across the wind turbine blade without any moving surfaces. Additional benefits of the PACE system include reduced blade structure weight and complexity that should translate into a substantially reduced initial cost.

During the Phase I program, the ORI-UND Team demonstrated (proof-of-concept) performance improvements on select rotor blade designs using PACE concepts. Control of both 2-D and 3-D flows were demonstrated. An analytical study was conducted to estimate control requirements for the PACE system to maintain control during wind gusts. Finally, independent laboratory experiments were conducted to identify promising dielectric materials for the plasma actuator, and to examine environmental effects (water and dust) on the plasma actuator operation.

The proposed PACE system will be capable of capturing additional energy, and reducing aerodynamic loading and noise on wind turbines. Supplementary benefits from the PACE system include reduced blade structure weight and complexity that translates into reduced initial capital costs.

1.1 Introduction

The recognition of the value of wind energy as a low cost, clean source for electricity is creating new business opportunities for manufacturing and materials innovation. Worldwide growth in wind power generation since 1994 has been 30% or higher annually [1]. However, the

wind power industry must still make substantial reductions in the cost per kilowatt hour to become competitive with fossil powered generating technologies. This can only come by improving wind turbine efficiency over a wider range of wind conditions and lowering construction costs. The cost of producing electricity from wind power is a function of the acquisition cost of the wind turbine system, lease or land purchase for the wind farm, transmission requirements to connect to the power grid, maintenance, and the amount of time the wind conditions are within the operational range of the wind turbine system. Each new generation wind turbine design has exploited improved technologies in blade aerodynamics, materials, controls, and generator innovations to lower system cost and expand the operational hours of the turbine per year.

These technologies all help in lowering the systems life cycle costs. In the 1970s, most horizontal axis wind turbines (HAWTs) used airfoils designed by the National Advisory Committee for Aeronautics (NACA) that were designed for the aviation industry. NACA airfoils were designed for airplanes that operate in a Reynolds number, Re, range much higher than that experienced by wind turbine blades. When such airfoils are used at lower Re, the airfoils suffered severe performance degradation from leading edge roughness contamination due to insect impact, or airborne pollutants. Tangler and Somers [2] discuss the evolution of airfoils used by the wind power industry. The aerodynamic performance loss using the NACA airfoil sections resulted in significant annual energy losses for wind turbines using these airfoils in their blade design.

In the mid-1980s, the National Renewable Energy Laboratory (NREL) as well as European research centers sponsored the development of a new family of airfoil sections designed to meet the needs of stall, variable pitch and variable rpm regulated wind turbines. Tangler and Somers [2] estimated that using the NREL airfoils would achieve annual energy improvements for stall, variable pitch, and variable rpm regulated wind turbines of (23-35%), (8-20%), and (8-10%), respectively.

The control of blade loading on large wind turbines also changed markedly in the last twenty years. Until the 1990s, most wind turbines were designed to control blade loading and power output using a passive control strategy of controlling the power output and rotor speed by stall regulation. In a stall-regulated turbine, as the wind speed increases the blades begin to stall. The increased drag makes the turbine less efficient thereby regulating the power extraction of the turbine. The large wind turbines designed in the 1990s use active control to

regulate rotor speed and power output by controlling the blade pitch angle of the turbine blades. Having the ability to control the blade pitch allowed for more efficient operation and blade load control. In addition, the use of active load control permitted designers the option to use lighter weight turbine blades.

The challenging issues facing the wind turbine designer include; regulation of the power output in high winds, providing a steady power output with time, and alleviation of large transient blade loadings. Phase I research show that plasma flow control technology offers the potential to improve wind turbine performance by expanding the operating wind range, controlling unsteady blade loadings, increasing blade fatigue life and reducing the noise of the wind turbine system. These benefits can be used to expand the operational time the wind turbine can be generating electricity. Increasing operational time allows more revenue to be generated by the turbine system and makes the machine more cost competitive with other electric generating technologies.

The most promising technology for making additional improvements in the control of blade aerodynamic loading is by applying "active flow control" technology in a distributed manner across each blade. Active Flow Control typically refers to the use of time-dependent (often periodic) disturbances that are introduced into the flow field by so-called "actuators." A system incorporating active flow control technology is one that includes flow actuators, flow sensors and control logic to use the sensor information on the state of the flow (separated or attached) and section loading to drive flow actuators to achieve a desired performance benefit. While there are a variety of flow control devices that could be used on a wind turbine; for example micro tabs, suction, blowing, synthetic jets and variable cambered airfoils using shaped memory materials, we believe that the dielectric barrier discharge (DBD) plasma actuator offers the greatest promise for wind turbine flow control.

The DBD plasma actuators have a number of distinct advantages over other active flow control devices for flow control on a wind turbine blade. The plasma actuators:

- are fully electronic with no moving parts,
- can withstand high force loadings,
- laminate into the turbine blade surface,
- require no slots or cavities,
- operate in both steady and unsteady modes,

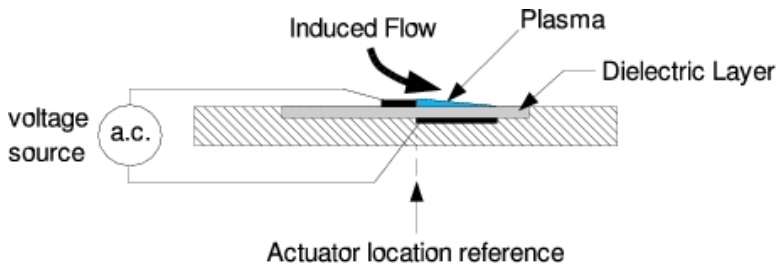

FIGURE 1: Schematic drawing of asymmetric electrode arrangement for plasma actuators.

- provide fast response time,
- consume low power (2-4 Watts per foot for unsteady operation).

1.2 Plasma-Enhanced Rotor Blade Aerodynamics

Plasma enhanced aerodynamics using dielectric barrier discharge (DBD) "plasma actuators" has been demonstrated in a range of applications involving separation control, lift enhancement, drag reduction and flight control without moving surfaces [3—14]. These actuators consist of thin electrodes separated by a dielectric insulator. One of the electrodes is typically exposed to the air. The other electrode is fully covered by a dielectric material. This asymmetric arrangement of plasma actuators is schematic illustrated in **Figure 1.** A high voltage a.c. potential is supplied to the electrodes. When the a.c. amplitude is large voltage enough, the air ionizes in the region of the largest electric potential. This generally begins at the edge of the electrode that is exposed to the air, and spreads out over the area projected by the covered electrode. The ionized air (plasma) in the presence of the electric field produced by the electrodes results in a body force on the ambient air. Details of the physics and mechanism of the plasma actuator are provided by Enloe et al. [15, 16]. Corke et al. [17] provide a recent general review of DBD plasma actuators.

The DBD plasma actuator has the property that it is self-limiting and therefore stable at atmospheric pressures. During the a.c. cycle, the electrons and ions move according to the sign in the alternating electric potential. As they move, the surface of the dielectric becomes charged. When the potential difference between the exposed electrode and the dielectric surface is large enough, the air over the dielectric layer ionizes. This continues until the charge on the dielectric surface builds up to the point that the potential difference is below the threshold for ionization and the process stops. This is the self-limiting aspect of the dielectric barrier that prevents a cascade of charges that would cause an electric arc, and distinguishes it from other approaches

that use an air gap between uncovered electrodes. With the DBD approach there is minimal heating of the air, and temperature change is not the mechanism for flow control. The body force is the mechanism for active aerodynamic control.

The body force vector can be tailored through the design of the electrode arrangement. Turbulent separation control can be achieved either by the injection of high momentum fluid, or by circulating high momentum fluid in the free-stream or outer part of the boundary layer towards the wall. The spanwise electrode arrangement which is often used in laminar separation control provides the former approach. The body force generated by this arrangement accelerates fluid towards the separation location to overcome the adverse pressure gradient. To enhance boundary layer mixing, a streamwise electrode arrangement was designed in order to generate a pair of counter-rotating vortices that are intended to circulate high momentum fluid from outer part of the boundary layer towards the wall to delay or suppress flow separation. It is important to note that from past demonstrations of active flow control, it appears that the success of active control strategies is greatest when hydrodynamic instability mechanisms of the underlying base flow can be exploited.

In addition to the experimental use of the plasma actuators, models for the space-time evolution of the plasma generation over the actuator, and a first-principle formulation for the body force produced by the plasma on the ambient flow, have been implemented in numerical flow solvers [18—20]. These have produced excellent agreement with experiments on leading-edge separation control in both steady and unsteady cases. Their purpose is to provide simulations that can be used in optimizing the design and placement of plasma actuators for different applications of flow control, for example like wind turbine blades, to enhance aerodynamic performance.

The further improvement in wind turbine aerodynamics and control will require active control technology to create a "smart" turbine blade. The most commonly used devices for controlling aerodynamic loading are leading-edge flaps or slats and trailing-edge flaps. **Figure 2** shows the aerodynamic changes created by each mechanical device. The leading-edge flap or slat extends the lift curve thereby increasing the maximum lift coefficient, C_{lmax}, and stall angle. A trailing-edge flap changes the effective camber of the airfoil and shifts the zero-lift angle of attack to negative or positive values depending on the direction of the flap (positive or negative) deflection. The trailing-edge flap is well suited for controlling the lift on any lifting surface and can be thought of as a "direct lift controller." Trailing-edge flaps have also been

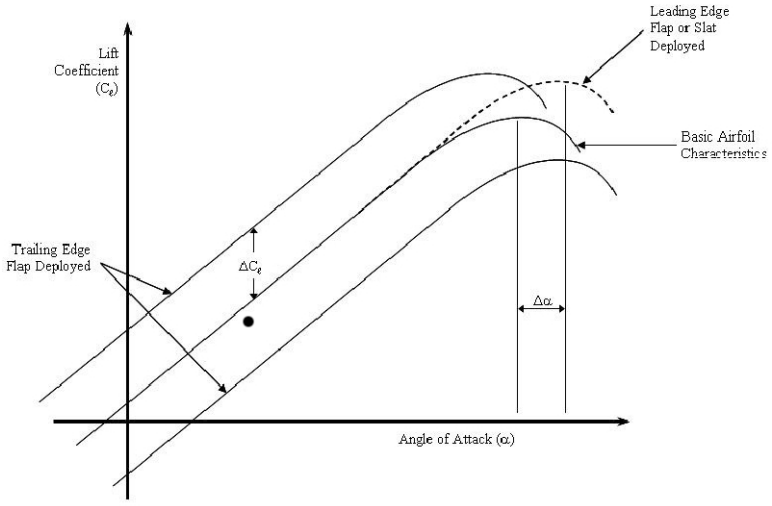

FIGURE 2: The aerodynamic changes created by leading and trailing edge flow enhancement devices.

examined for wind turbine control applications [21, 22]. While these studies showed that trailing-edge flaps were effective in controlling the power output and providing blade load mitigation, the major disadvantage of mechanical flaps is their complexity, added structural weight (linkages, support structure, actuators, etc.), time delay in response and additional maintenance. The disadvantages of mechanical flaps could be avoided if flow control devices without moving surfaces, like the plasma actuators, were used. In the following section we will highlight the potential benefits of active flow control technology in the form of plasma flow actuators for wind turbine applications.

1.3 Smart Turbine Blade Concept

New wind turbine designs include the capability of changing the blade pitch to improve energy extraction. In a steady wind condition, the power extracted can be achieved by optimizing the blade pitch angle by rotating the blade within the turbine hub. Further improvements in performance can be achieved by controlling each blade individually. In this control scheme, the entire blade is rotated to obtain the best power extraction for the given wind conditions. While this is an improvement over a fixed pitch blade, the blade can still experience regions of stall and unsteady loading during each rotation. To achieve an optimum performance improvement in a velocity field that varies both spatially and temporally across the blade, one would need to be able to adjust the local blade pitch angle across the turbine blade. The distribution of active flow control can be used to optimize the wind power extraction of the system and to moderate the blade loading across the span of the blade.

In unsteady wind conditions, the problem is one where the local spanwise pitch needs to be changed. Distributed flow control permits local aerodynamic load control that is equivalent to an effective local pitch angle change. The change in the flow field gives rise to what we call virtual shaping of the airfoil section. Virtual shaping is the modification of the flow field around the surface by means of flow control (plasma actuators), which results in flow changes as if the geometry itself is altered. By incorporating the distributed flow actuators, sensors with the appropriate control logic one can envision the possibility that multiple control objectives could be accomplished. **Figure 3** is a sketch showing a simple arrangement of plasma actuators distributed near the leading-edge and trailing-edge. The basic idea is to divide the blade into regions that can be individually controlled. The spacing of actuators and number of sections

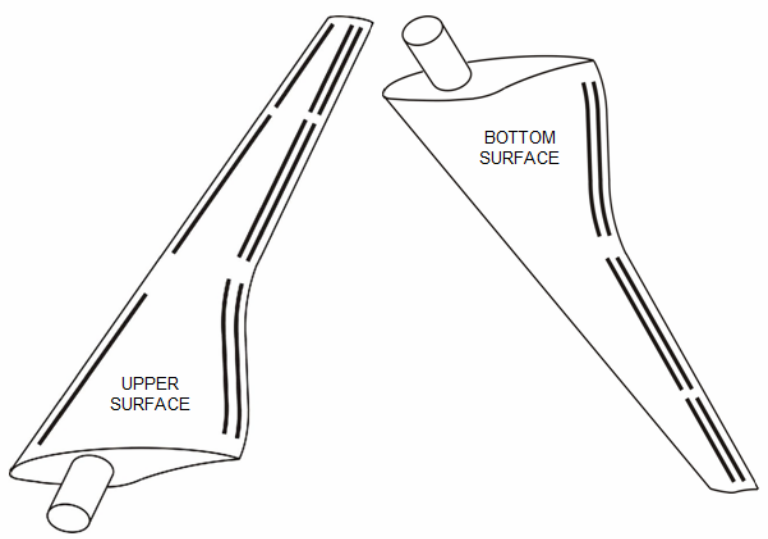

FIGURE 3: Example of distributed DBD flow control actuators on wind turbine blade. The rotor blade shown is a generic representation of a small/large wind turbine.

would be determined by the desired control function. The virtual trailing-edge flap actuators would be located on both upper and lower surface of the airfoil section.

A paper by G. van Kuik, T. Barlas, and G. van Bussel [23] outlined the need for improved blade control concepts for the next generation of large wind turbine designs that are expected to enter service in the year 2020. They presented an overview of various control technologies that could be used to design a smart turbine blade. A truly smart turbine blade would use distributed sensors, flow control actuators and a supervisory controller to select the appropriate control logic for using the flow actuators. The supervisory controller would select different control logic depending on the needed control, i.e., blade loading control, blade stall prevention, or braking

torque for emergency shut down. The point here is that distributed control gives the designer the potential for optimally controlling a variety of wind turbine control tasks. **Table 1** provides a summary of some of the potential benefits afforded by distributed plasma flow actuators.

Table 1: Potential advantages of Distributed Virtual Plasma Slats and Flaps.

Benefits of the PACE Technology	*Wind Turbine Improvement*
Distributed Virtual Plasma Flaps are used to control large transient loads due to unsteady steady wind conditions.	Controlling transient blade loading low-blade root bending moment transients. *This will improve turbine blade fatigue life and allows operation over a wider range of wind conditions.*
Distributed Virtual Plasma Flaps are used to control rotor speed.	Emergency shut down requires redundant control capability. Virtual-slats and flaps will be used to help brake the turbine by provide braking torque. *This will provide greater control flexibility.*
Distributed Virtual Plasma Flaps allow larger span turbine blades.	Turbine blades of greater span can be designed if load control is available to attenuate transient blade loading due to unsteady wind conditions. *Increasing blade span permits greater energy extraction.*
Wind turbine spacing is governed by wake flow interference between wind turbines in the wind farm. Distributed Virtual Plasma Flaps have the potential to allow more efficient turbine performance from down wind turbines.	Virtual Plasma Flaps allow improved energy extraction from down wind turbines by optimizing the aerodynamic loads across the blades. Will allow more wind turbine to be placed on a given track of land than is currently possible.
Distributed Virtual Plasma Slats control C_{lmax} that will allow improved performance - on stall regulated wind turbines. It will also be useful in turbine startup.	Virtual Plasma Slats will be used to control blade section C_{lmax}.

2. Anticipated Public Benefits

Numerous economic, social and technical benefits will be realized upon successful implementation of the PACE system which includes innovative actuators, sensors and intelligent control. Alternative energy sources such as wind, solar, and geothermal provide specific options and advantages over the conventional power grid, but must be economically competitive to be accepted. Since 1980, the cost of power from wind farms has dropped from 38 cents to 4 to 7 cents per kWh, and it continues to decline. The cost of wind energy is now on a par with the cost of coal and gas, and it is cheaper than nuclear. Multiple drivers exist for wind energy, including in part:

- construction of wind turbines take months, not years;
- wind turbines can be added in small increments to match growth in demand;
- wind energy creates 27% more jobs than advanced coal technology and twenty times more jobs than natural gas combined cycle—customers pay for people, not fuel;
- wind energy can be available in remote locales;
- only a tiny fraction of the wind energy potential market has been tapped.

The two financial components that comprise a wind system are the initial installation costs (capital) and operating costs. Orbital Research's PACE system will dramatically impact the acceptance of wind systems by: (1) minimizing the capital costs by reducing the need for over design in the turbine and, (2) increasing the net efficiency of operation of the system by virtually shaping the blades.

Ultimately, the social benefits of wind energy will be most noteworthy. These benefits include a reduction in sulfur and nitrogen oxide emissions (acid rain) along with carbon dioxide (greenhouse effect). When coupled with other alternative energy sources, the impact of wind energy on the planet's environment and the health of its inhabitants will be profound and positive.

Nationwide, as many as 30,000 deaths a year are related to power plant emissions, according to a study by Abt Associates, a private research organization that does work for the EPA. By comparison, 16,000 Americans are killed each year in drunken driving accidents, and more than 17,000 are victims of homicides. (Source: Washington Post 3/6/02).

In addition to reduced emissions, increased adoption of wind energy will dramatically reduce the drain on non-renewable natural resources such as coal, gas, and oil. The more subtle, long term strategic impact of the application to wind energy will be decreased dependence on foreign energy sources.

Besides improvements in efficiency, the technology improvements imparted by PACE will also permit a significant reduction in the acoustic signature that present wind turbines are known for, i.e. the wind turbines will operate much more quietly. Technological solutions will also have noteworthy impact on government agencies and business areas outside the scope of wind energy. Applying this nascent plasma based microactuator technology to aerodynamic systems will greatly benefit next generation manned and unmanned aircraft control. Additional applications exist for noise reduction in turbine engines as well as improving the combustion efficiency through controlled air flow. For the wind turbine industry, the PACE system can be designed into a new generation of rotors, or, provided in kits that could be retrofitted onto existing rotors.

3. Phase I Accomplishments

Several wind tunnel experiments, numerical computations, and plasma actuator characterization studies were conducted during the Phase I program to demonstrate the technical feasibility of the proposed PACE concept for improved wind turbine performance. Three rotor blade models were constructed and integrated with plasma actuators in various configurations to test aerodynamic flow control strategies for improved blade characteristics. Measures of performance included ability to control 2-D and 3-D flow separations over the blade models, increment in C_l over a range of angles of attack on blades without any moving surfaces, and ability to alleviate wind gusts using plasma actuators. Additionally, laboratory experiments were conducted to examine the effects of (simulated) rain and dust on the plasma device operation, results from which were recorded using a digital video recorder, and an oscilloscope that measured the resultant changes in the actuator voltage, current and frequency. A quick summary of all major technical accomplishments during the Phase I are listed below. Additional details of significant feasibility demonstrations are provided in the subsequent sections. It should be noted that we revised (and also expanded) the Phase I objectives and the technical scope, compared to what was originally proposed, based on the feedback received from the Technical Monitor and experts from NREL and Sandia Research Laboratories during the Phase I kickoff meeting.

Objective 1: Design and construction of rotor blade models to demonstrate the technical feasibility of the PACE concept in a wind tunnel.

- **Accomplishment:** After examining several candidate rotor blade designs and through consultations with engineers from Sandia National Laboratory and National Renewable Energy Laboratory (NREL), two airfoil profiles, S827 and S822, were chosen for the Phase I feasibility study. A total of three airfoil models: 1) a modified 2-D S822, (2) a 2-D S827, and (3) a 3-D S827 were designed, fabricated and instrumented with plasma actuators for experimental study.

Objective 2: Design, integrate and test plasma actuator configurations on blade models to demonstrate performance improvement using flow control techniques. Performance improvement to be measured in terms of increasing C_l on a blade, which translate into improved power capture.

- **Accomplishment**: Wind tunnel experiments were conducted on two blade

models (2-D S827 and modified 2-D S822) to demonstrate an enhancement in blade characteristics. Aerodynamic improvements were achieved by changing the blade circulation using a trailing-edge plasma actuator on a 2-D S827 blade model and by controlling flow separation on a 2-D modified S822 blade model.

Objective 3: Investigate the use of plasma to control 3-D effects, typical of flow fields over a wind turbine blade.

- **Accomplishment**: Wind tunnel experiments were conducted on a 3-D, twisted S827 model (with 7°/m spanwise twist) to demonstrate control of 3-D flow separation over the blade model. A novel, streamwise plasma actuator configuration that act as a "vortex generator" was used on the leading-edge of the airfoil to reattach 3-D flow separation. Aerodynamic improvements were achieved by controlling leading-edge flow separation.

Objective 4: Conduct numerical studies to model the effects of plasma actuators on a select rotor blade model. Validate the modeling data by comparing with experimental data.

- **Accomplishment**: A CFD study was conducted using a Navier-Stokes flow solver that modeled the effects of a plasma actuator on a 2-D S827 model, same airfoil and actuator configurations that were examined in a wind tunnel. Numerical results are in good agreement with the wind tunnel test results, thus validating the plasma model.

Objective 5: Estimate the amount of change plasma actuators would have to create on a blade model in order to maintain control (constant lift) in the presence of wind gusts. This portion of the study focuses on the ultimate use of plasma actuators for gust load alleviation.

- **Accomplishment**: An analytical study was conducted to investigate effect of gust loads on airfoil lift in order to identify delta C_l required to maintain control. The effect of gusts on effective angle of attack and wind speed was incorporated into the analytical model. The ultimate goal of this study is to develop a plasma actuator configuration, or configurations, that can generate the required delta C_l to maintain control (constant lift) in the presence of gusts. Quantified control requirements on a 2-D rotor blade model for varying gust conditions.

Objective 6: Investigate environmental effects on the plasma actuator operation. In particular, effects of water (to simulate rain), and dust/sand (to simulate dirt).

- **Accomplishment**: In-house laboratory experiments were conducted to study the effects of water and dust on the plasma actuator operation. Fatigue tests were also conducted where the tests were run over 30 minutes with repeated exposure to rain and dust. Results demonstrate the actuator temporarily shuts off under fully soaked conditions and resumes operation once the water molecules are pushed off. Since water does not accumulate on a rotating blade, the operation of the plasma actuator will not be affected. We believe this Sand/dust has no affect whatsoever on the plasma actuator. No performance degradation is observed under both conditions. Data is captured using a digital video recorder.

Objective 7: Discuss plasma actuator material selection and a method of integration onto a wind turbine blade model.

- **Accomplishment**: Laboratory tests were conducted to test the performance of several candidate dielectric materials. Promising dielectric materials were identified and reason for improved performance was established. A robust design approach to implement a plasma actuator onto a wind turbine model was developed.

4. Plasma-Induced Blade Circulation Control on 2-D S827 and S822 Models

The objective of these wind tunnel experiments was to demonstrate the feasibility of using plasma actuators to achieve control of aerodynamic lift on select 2-D blade models at low angles of attack, much like the effect produced by circulation control or a wing camber, but without using any moving surfaces. The experiments were conducted in a subsonic wind tunnel. The wind tunnel used was a low turbulence, in-draft (open-return) design. The test section has a square cross-section of 2 ft x 2 ft (0.61 m x 0.61 m) and a test section length of 6 ft (1.8 m). The tunnel is capable of producing velocities in a range of 5 to 35 m/sec, with a turbulence level of 0.08% over the velocity range.

The 2-D airfoil models were mounted vertically using a sting connected to a lift and drag force balance located on the top of the test section. End-plates were mounted to the test section ceiling and floor to produce approximately 2-D flow over the airfoil. The end-plates were secured to the walls of the test section and were separated from the airfoil by a small gap. A schematic of the force balance and test section is shown in **Figure 4**.

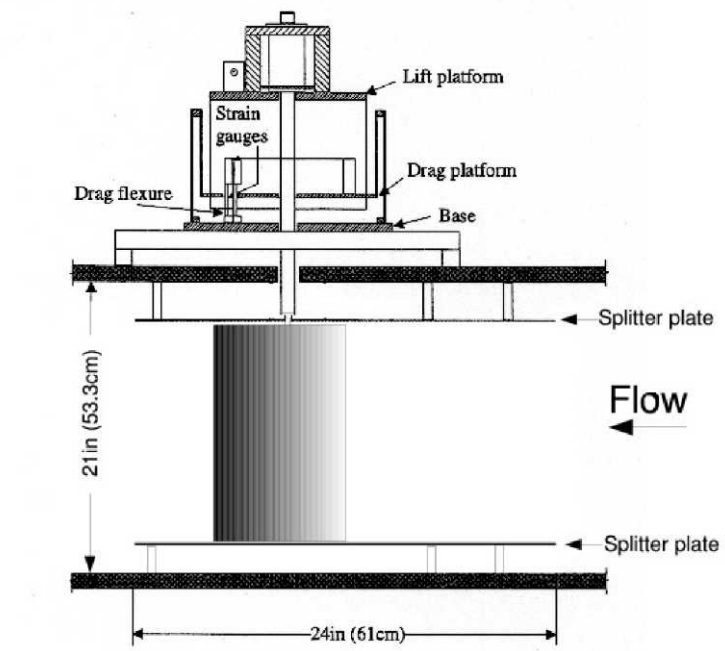

FIRURE 4: Schematic of experimental setup used for measuring lift and drag at different angles of attack on turbine blade sections.

Two airfoil profiles designed for wind turbine applications were selected for this study. These were the S827 [24] and the S822 [25] profiles. The section shape for the S827 airfoil is shown in **Figure 5**. The section shape for the S822 is shown in **Figure 6**, where the solid curve is the baseline shape and the dashed curve shows the shape as modified to add flow separation ramps at the trailing-edge.

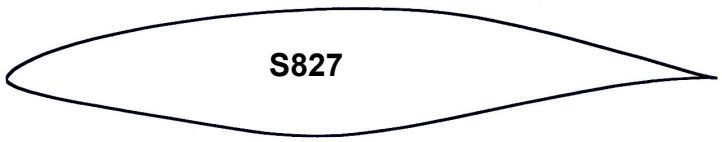

FIGURE 5: Section shape of S827 airfoil used in DBD flow control experiments.

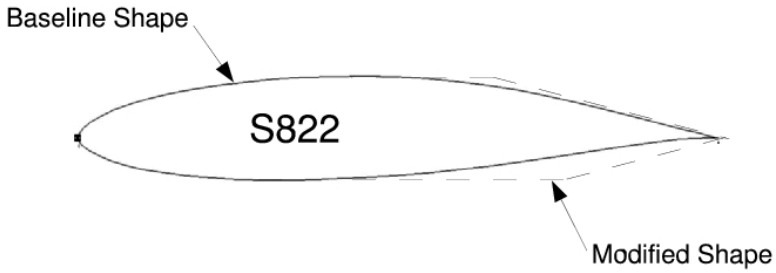

FIGURE 6: Section shapes of baseline S822 airfoil (solid curve) and modified shape (dashed curve) to add flow separation ramps.

4.1 Experimental Results

Experiments were performed on both airfoil shapes to determine the effect of placing DBD plasma actuators in different configurations and locations on the lift and drag. The objectives for the two profile shapes were different. For the S827 section shape, the objective was to use steady plasma actuators that have been shown to provide circulation control that is equivalent to increasing the effective camber [9, 28, 29].

For the S822 section shape, the objective was to modify the profile to produce flow separation ramps that could be manipulated by the plasma actuators to produce different pressure distributions near the trailing-edge. The advantage of this approach is that it can be accomplished with unsteady plasma actuators that can potentially use only 10% of the power of the steady plasma actuators.

The airfoils were cast from molds that were machined using a numerically controlled milling machine. The casting material consisted of a two-part epoxy that was mixed with micro-glass spheres. The resulting airfoils were extremely rigid, with a smooth hard surface.

4.1.1 2-D S827 Profile:

Both spanwise and streamwise plasma actuator configurations were investigated in this study. The spanwise plasma actuator configuration was based on the asymmetric configuration that was shown in Figure 1. The electrodes were made from copper foil tape. The dielectric material was Teflon sheet. The Teflon was recessed into the airfoil so that the exposed surface was flush with the surface of the airfoil. The edges of the electrodes were aligned in the spanwise direction. They were overlapped by a small amount (of the order of 1 mm), in order to ensure a uniform plasma in the full spanwise direction.

The experiments were conducted at a 20 m/s freestream speed. The actuator ran in steady operation. The frequency of the a.c. voltage supplied to the electrodes was approximately 2.3 kHz. The precise frequency was tuned to maximize the body force and minimize ohmic heating [20]. The actuator a.c. waveform was a saw-tooth wave, which has been shown to produce the maximum body force [15].

Figure 7 shows the lift coefficient versus angle of attack for the baseline S827 airfoil and with the DBD plasma actuator at x/c = 0.78 operating. The range of angles of attack corresponds to the linear range of C_l versus α. The baseline values correspond to the open circles. The solid line through these points corresponds to a best-fit straight line. The slope of the line is approximately 0.11/° which agrees with linear theory.

The plasma actuator was designed to induce a wall jet in the mean flow direction. This had previously [9] been shown to increase the lift at a given angle of attack that was similar to increasing the airfoil camber or, the positive deflection of a plane trailing-edge flap. The lift coefficient versus angle of attack for the S827 with the plasma actuator on is shown as triangles in Figure 7. The dashed line corresponds to a best-fit straight line through these points. The slope, $dC_l/d\alpha$, is approximately the same as the baseline, as we expect based on simulations to be discussed in a later section. In this case, we note a positive shift in the lift coefficient of approximately ΔC_l = 0.08. This corresponds to a change in the equivalent angle of attack of approximately $\Delta\alpha$ = 0.7°. This is equivalent to a 2° deflection of a plane flap having a C_f/c = 0.10 [30]. As mentioned earlier, such flaps are sometimes used for lift control [21, 22], however

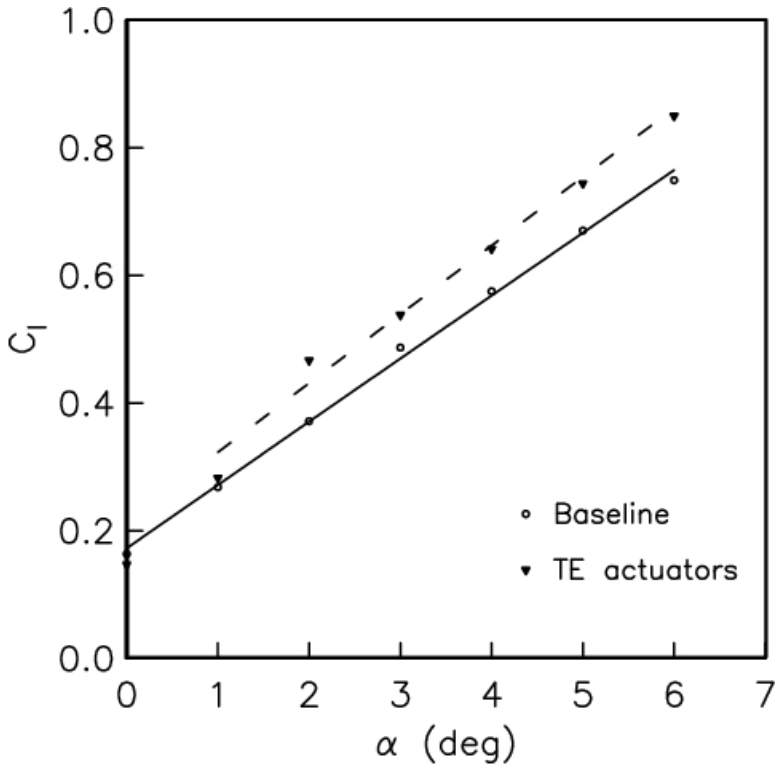

FIGURE 7: Comparison of lift versus angle of attack for baseline S827, and with spanwise oriented plasma actuator at *x/c* = 0.78 operated to produce effective increase in camber.

they add complexity and weight to the rotor. A trailing-edge plasma actuator for lift control has the advantage of adding insignificant weight as well as having faster response for dynamic gust control.

The trailing-edge control was intended for the linear C_l versus a range of angles of attack. However, it is possible to apply them near the leading edge of the airfoil to increase the stall angle of attack and increase C_l max. We have generally done this using spanwise oriented electrodes like the trailing-edge actuator just presented (see for example Post [6,7]). However, we [31, 32] recently have used plasma actuators that were designed to act as streamwise vortex generators. These are intended to mimic the effect of delta-shaped tabs by generating streamwise-oriented counter-rotating vortices.

A schematic illustration and photograph of the streamwise plasma actuators near the airfoil leading edge and operating in a darkened lab are shown in **Figure 8**. The covered electrode ran across most of the span of the airfoil model. The spanwise spacing (z) between the exposed electrodes is an important parameter to optimize their effect [31, 32]. This should scale with the boundary layer thickness at the chordwise location where the streamwise vortex generating

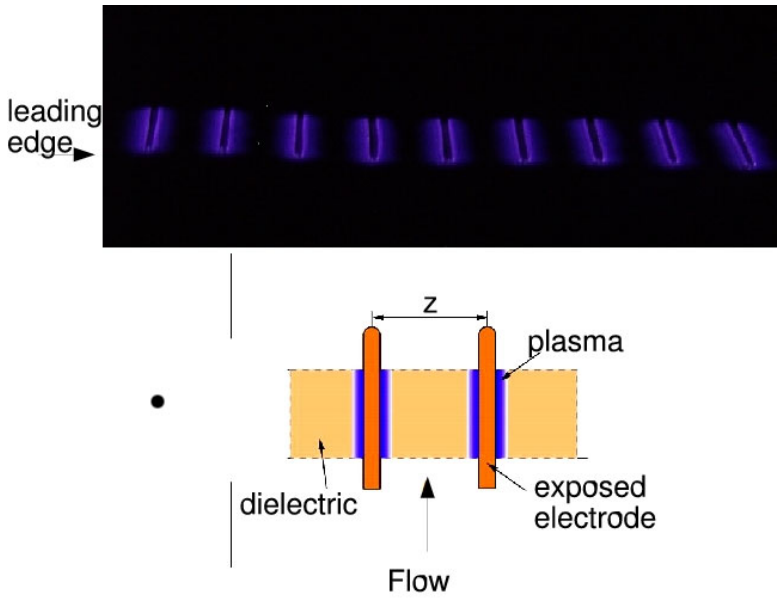

FIGURE 8: Photograph of streamwise plasma actuators operating in a darkened lab (top); schematic illustration of streamwise vortex generating plasma actuators (bottom), and photograph of streamwise plasma actuators operating in a darkened lab (top).

plasma actuators are placed.

The effect of the streamwise vortex generating plasma actuators on the lift characteristics of the airfoil at near-stall angles of attack are shown in **Figure 9**. The conditions for these

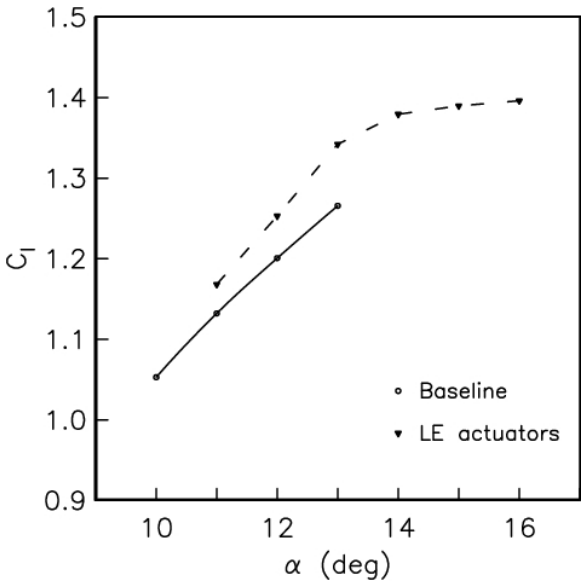

FIGURE 9: Comparison of lift versus angle of attack for baseline S827, and with streamwise oriented plasma actuators covering 0 < *x/c* < 0.2 designed to produce counter-rotating streamwise vortices. .Note a = 13° was limit for baseline measurements due to violent shaking of model at higher angles of attack.

measurements are identical to those with the trailing-edge actuator. As before, the baseline values correspond to the open circles. The solid line through these points corresponds to a smooth spline that was added to guide the eye. The 13° angle of attack was the highest that could be achieved because of violent shaking of the model due to unsteady loads produced near stall of the airfoil.

The triangle symbols correspond to the results with the streamwise vortex generating plasma actuators. The dashed curve corresponds to a smooth spline that again is intended to guide the eye. The leading-edge plasma actuators increased the lift coefficient for larger angles of attack greater than 11°. In addition, it significantly extended the stall angle of attack, which allowed measurements well beyond the 13° limit encountered with the baseline airfoil.

4.1.2 2-D S822 Profile:

For the S822 section shape, the objective was to demonstrate control at low angles of attack using flow separation ramps at the trailing edge that could be manipulated by the plasma actuators to produce different pressure distributions. The motivation for this approach was that it could provide lift control with unsteady plasma actuators that could potentially use only 10% of the power of the steady plasma actuators used for lift control.

The baseline and modified section shapes were shown in Figure 6. The ramp sections were linear cuts having angles of 15° with respect to a line tangent to the surface at the airfoil maximum thickness point. The addition of the ramps required a slight flattening of airfoil profile near the maximum thickness location. This was done so that the overall length of the airfoil would remain the same as the baseline. A more dramatic flattening of the pressure side (lower surface) of the airfoil was needed to accomplish the addition of the ramp. The addition of these ramps was in no means optimized. The intention was to insure that the flow would separate at the trailing edge for the range of angles of attack where the baseline airfoil produced positive lift.

The experiments with the S822 airfoil were conducted at a free-stream speed of 14.5 m/s, which corresponded to Rc = 0.303 X 106. The lift characteristic for the baseline S822 airfoil and the effect of the passive ramps are documented in **Figure 10**. The baseline S822 airfoil (circle symbols) has a well defined linear C_l versus a region. The solid line in the plot corresponds to a best linear fit through this region. The slope is approximately 0.11/° which we expect from linear airfoil theory. As opposed to the S827 airfoil, we were able to include angles of attack

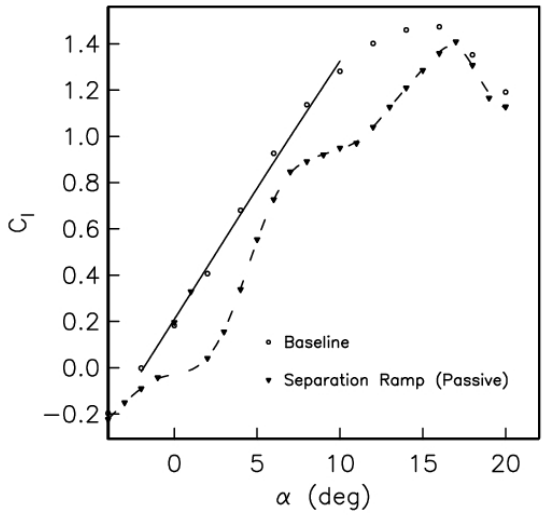

FIGURE 10: Comparison of lift versus angle of attack for baseline S822 and modified S822 having passive trailing edge separation ramps.

through stall without violent vibrations. The S822 exhibits a well defined stall angle of attack of 16° which is followed by a relatively fast drop off in lift.

The lift versus angle of attack for the modified S822 is shown by the triangle symbols in **Figure 10.** The dashed line through the points is a spline curve that is intended to guide the eye. At lower angles of attack, the lift coefficients fall below the baseline values. The amount that it falls below varies with angle of attack, with maximum deviations occurring at approximately a = 3° and 11°. At these angles of attack, the difference between the baseline and modified lift coefficients is approximately $\Delta C_l = 0.4$.

Suction-side Ramp: Flow visualization was performed to verify that the flow was separated over the suction-side ramp. A sample flow visualization record is shown in the top photograph in Figure 11. The flow visualization was performed by introducing a sheet of particle streak lines upstream of the airfoil. The sheet is perpendicular to the airfoil surface. The sheet of particles was illuminated using a 5W Argon laser whose coherent beam was passed through a cylindrical lens to produce a thin sheet of light. The light sheet illuminated the mid-span location of the airfoil as illustrated in the right half of **Figure 11.**

The top image in Figure 11 documents the flow over the suction-side separation ramp with the airfoil at a = 3°, which is where one of the maximum deviations occurred in C_l between the baseline and modified S822 airfoils. The flow visualization at this condition reveals a large separation bubble over the separation ramp.

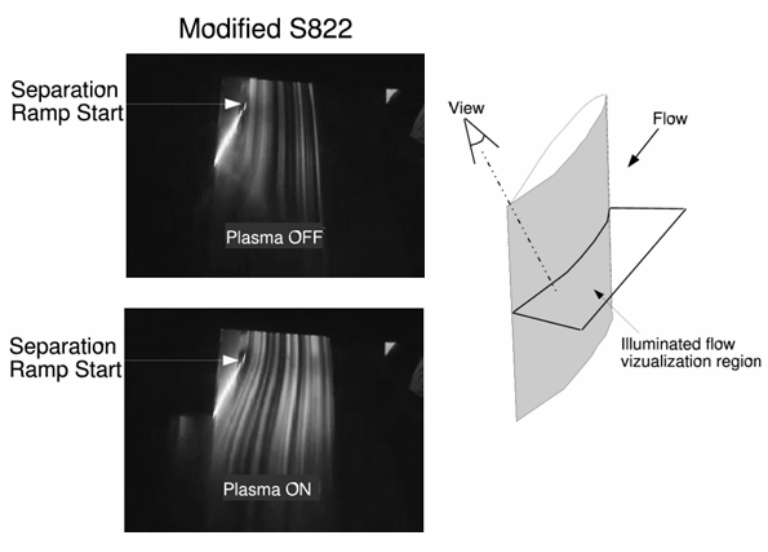

FIGURE 11: Flow visualization over suction-side trailing-edge ramp of modified S822 airfoil with plasma actuator off (top) and on (bottom). Right illustration shows orientation of visualized segment of flow.

A spanwise-oriented plasma actuator with an asymmetric electrode arrangement like that illustrated in Figure 1 was used to control the flow separation over the ramp. This actuator design was identical to that used at the trailing edge of the S827 airfoil for circulation control. In this case, the actuator was located just upstream of the separation ramp. In addition, the actuator was periodically turned on and off at a frequency, *f*. The frequency was chosen so that JCr/UOQ = 1, where Cr is the chord length of the ramp. This frequency scaling based on the separation length and free-stream velocity has been shown to be optimum for separation control [5].

The bottom image in Figure 11 documents the flow over the ramp with the plasma actuator ON. This indicates a complete re-attachment of the flow. The effect of the plasma actuator on the lift characteristics of the modified S822 airfoil are documented in **Figure 12**. This shows the lift coefficient versus angle of attack for the baseline airfoil (circles), the modified airfoil (dashed curve), and the modified airfoil with the plasma actuator reattaching the flow over the ramp on the suction side of the airfoil (triangles). With the actuator operating, the lift in the region $-3° < a < 5°$ is increased. For $-3° < a < 3°$, the lift characteristics of the baseline airfoil are recovered with the plasma actuator. Above $a = 7°$, the separation control over the trailing-edge ramp had no effect. Flow visualization in this case indicated that the flow was separated at the airfoil leading edge. Therefore the addition of leading-edge plasma actuators similar to that used in with the S827 could be used here to improve the lift characteristics at the larger angles of attack. The modified S822 for provided improved lift control over a range of angles of attack

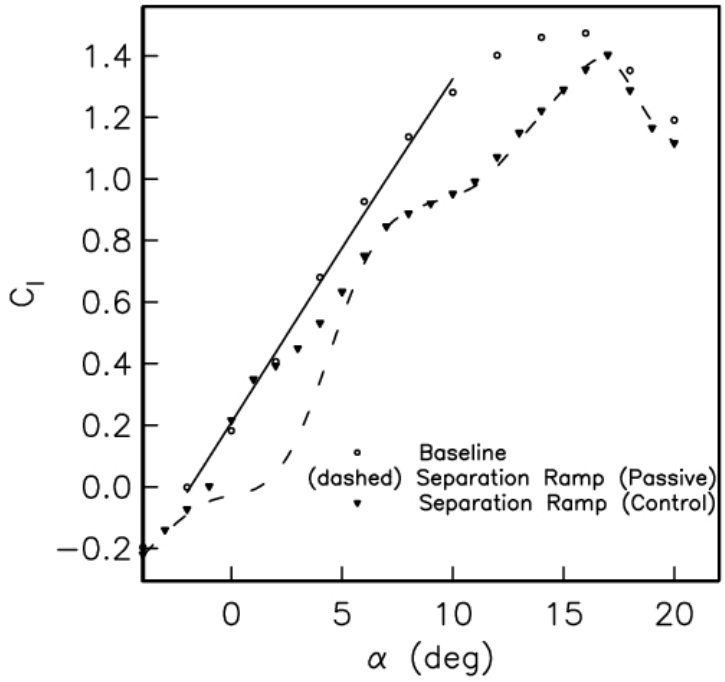

FIGURE 12: Comparison of lift versus angle of attack for baseline S822 (circles) and passive modified S822 (dashed curve) and modified S822 with plasma actuator on suction-side separation ramp (triangles).

compared to the circulation control used for the S827 airfoil.

Pressure-side Ramp: In some wind turbine applications there is a desire to reduce the lift on the rotors. This is generally the case when the wind speeds are excessive and could lead to damage to the rotor blades. The separation ramp on the pressure side of the modified S822 airfoil was intended for this application.

The effect of the separation control of the pressure-side ramp of the modified S822 airfoil is documented in **Figure 13**. This shows the lift coefficient versus angle of attack for the three cases corresponding to the passive modified S822 airfoil (dashed curve), the modified S822 with plasma actuator operating at the suction-side separation ramp alone (triangles), and the modified S822 with plasma actuator operating at the pressure-side separation ramp alone (circles). The data for the passive modified S822 airfoil and the case with the plasma actuator operating at the suction-side separation ramp are same as that presented in Figure 12. These were included for reference in the smaller highlighted range of angles of attack displayed in the figure. In contrast to the suction-side flow control which increases the lift coefficient when the

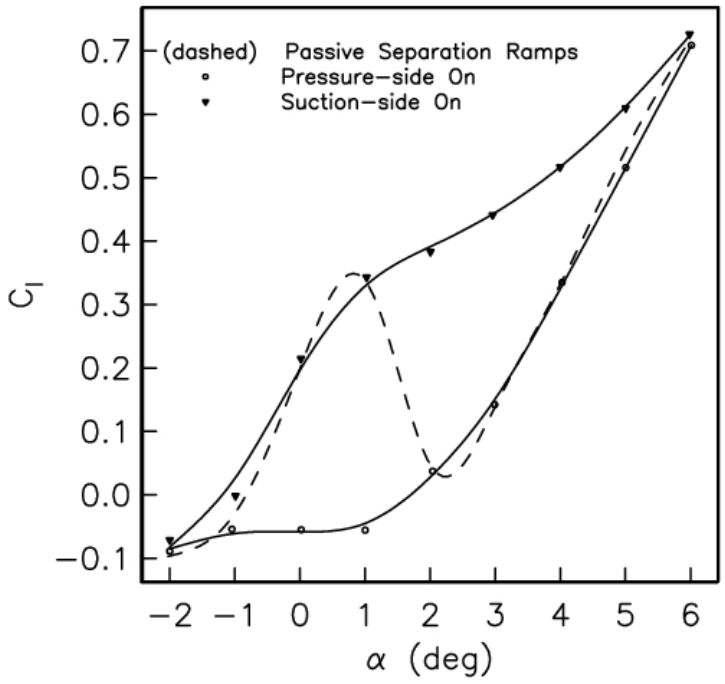

FIGURE 13: Comparison of lift versus angle of attack for the passive modified S822 airfoil (dashed curve), the modified S822 with plasma actuator operating at the suction-side separation ramp alone (triangles), and the modified S822 with plasma actuator operating at the pressure-side separation ramp alone (circles).

flow is attached, the flow control on the pressure side decreases the lift coefficient when the flow is attached over the ramp. At a = 1°, the change in the lift coefficient was approximately -0.4, which was comparable to the positive change in the lift coefficient achieved with the suction-side ramp control. The combination of these two gives a great deal of flexibility to tailor the lift over a range of angles of attack.

4.2 Discussion of 2-D Blade Model Test Results

For the modified S822 airfoil, general concept was to demonstrate the use of a plasma actuator to produce effects similar to adding camber to the airfoil. This is done by controlling flow separation near the trailing edge using a plasma actuator. This approach was first tried by us [26] on an HSNLF(1)-0213 (natural laminar flow) airfoil, which has a concave trailing-edge section where a separation bubble forms. A more general approach is to design airfoil section shapes that are optimized to be highly receptive to flow control for lift control without moving surfaces. An example of that approach was presented by Nelson et al. [27].

In the present approach, the plasma actuators were shown to recover the lift coefficient of

the baseline shape on the modified S822 airfoil. This could be used to moderate the span-wise lift distribution on a wind turbine blade to maintain a spanwise-uniform aerodynamic loading. By combining with leading-edge plasma actuators, the overall performance of the modified S822 airfoil would be improved beyond the baseline.

Although the addition of a separation ramp looks promising for lift control on airfoils used in wind turbines, circulation control demonstrated with the S827 airfoil has some unique advantages as well. Hall [28,29] examined the effect of the chord location of a plasma actuator on the enhanced lift it produced. This involved an inviscid simulation in which the effect of the plasma actuator was modeled as a doublet (source-sink combination). In the simulation, the doublet strength was fixed and determined by comparison to an experiment. Hall verified that based on one comparison experiment at one angle of attack and actuator input voltage, the simulation agreed with the lift over a range of angles of attack for the same and different free-stream speeds. This simulation only applies to thin airfoils in the linear C_l versus a range where no flow separation is present.

Figures 14 and 15 are from Hall [28,29] and were based on a NACA 0015 airfoil. Although these are different section shapes than those examined in this SBIR program, the fundamental physics is expected to be the same.

Figure 14 shows the change in the lift coefficient multiplied by the square of the free-stream speed, versus the angle of attack and x/c location of a single plasma actuator. For a given angle of attack, the change in the lift increases as the actuator moves towards the trailing edge. An actuator placed near the leading edge is slightly less effective with increasing angles of attack, although angle of attack sensitivity decreases as the actuator moves towards the trailing edge.

Figure 15 shows the change in the lift coefficient for a free-stream speed of 20m/s (the value used in the present experiments with the S827 airfoil where this analysis applies) for different actuator locations and angles of attack. In the present experiment, the actuator was placed at x/c = 0.78. For the input voltage used, this produced a ΔC_l = 0.08. According to Figure 15 at this chord location, the effect of angle of attack on ΔC_l is minimal. The value of ΔC_l in the present experiment was approximately 2.7 times that given by Hall [29]. However, the plasma actuator used in determining the doublet strength produced a significantly lower body force (see Iqbal [33]) by an amount that corresponded to the ratio of ΔC_l values. If we were to simply re-scale ΔC_l values in Figure 15 [29] it would provide an indication of the effect of the present plasma actuator for lift control.

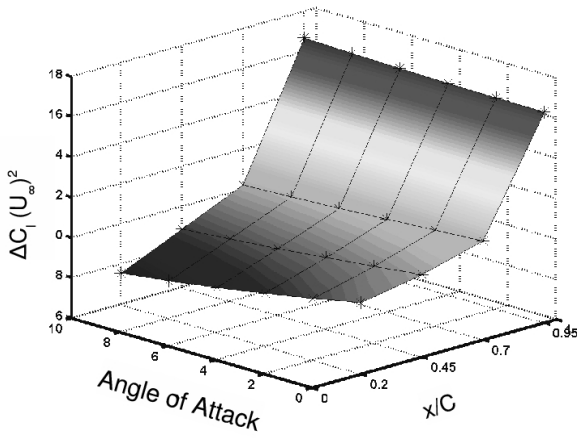

FIGURE 14: Change in lift versus plasma actuator *x/c* position and airfoil angle of attack. (From Hall et al., 2005 [29])

Since the effect of multiple plasma actuators is additive, Figure 15 provides a guide for digital lift control of the turbine rotor airfoil sections. For example if an actuator of present design located at x/c = 0.9 were operated simultaneously with the one at x/c = 0.78, the combined lift enhancement is predicted to be ΔC_l = 0.08 + 0.099 = 0.18. If another actuator is added at x/c = 0.6, the total ΔC_l = 0.23. The total lift enhancement produced by three plasma

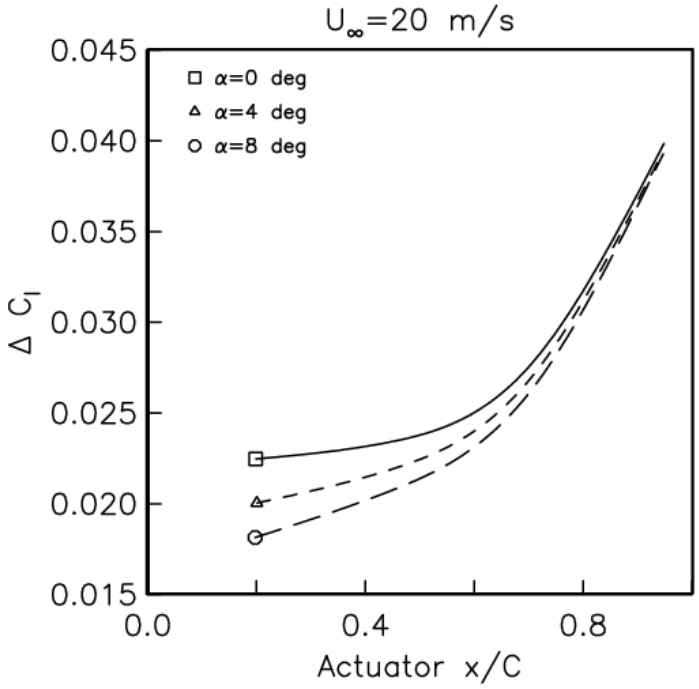

FIGURE 15: Change in lift versus plasma actuator *x/c* position at different airfoil angles of attack for U_∞ = 20 m/s. From Hall et al., 2005.

actuators operating simultaneously would provide the equivalent of a 5.5° flap deflection of a trailing-edge flap with C_f/c = 0.1. The digital control comes by operating multiple numbers of actuators in different combinations to generate discrete changes in lift in response to dynamically changing conditions. This is the premise behind the PACE rotor concept that was shown in Figure 3.

4.3 Summary of 2-D Blade Model Test Results

DBD plasma actuators were demonstrated in experiments to provide lift control on two wind turbine blade section shapes designated S827 and S822. For the S822 section shape, the objective was to demonstrate control at low angles of attack using flow separation ramps at the trailing edge that could be manipulated by the plasma actuators to produce different pressure distributions, and thereby control the overall lift. The ramp sections were linear cuts having angles of 15° with respect to a line tangent to the surface at the airfoil maximum thickness point. The overall length of the airfoil would remain the same as the baseline.

Without separation control at the ramps, the lift distribution with angle of attack of the modified S822 airfoil fell below the baseline values. The maximum deviations occurring at approximately $\alpha = 3°$ and 11°. The deviation at the smaller angles of attack were due to the flow separation over the ramps. At the higher angles of attack, the deviations were due to a premature leading edge separation. The plasma actuator could recover the lost lift at the lower angles of attack between $-3° < \alpha < 3°$. In this range, the maximum change in lift between having the plasma actuator on and off was approximately $\Delta C_l = 0.4$. This is equivalent to a 10° deflection of a plane trailing-edge flap with a $C_f/c = 0.1$. This was performed with a periodically pulsed plasma actuator which reduced the power to the actuator by 90% over steady operation used for lift control based on circulation control.

For the S827 section shape, the objective was to demonstrate the use of steady plasma actuators to generate the effects equivalent to increasing the effective camber of 2-D airfoil sections using circulation control. The actuator resulted in a positive shift in the lift coefficient of approximately $\Delta C_l = 0.08$. This corresponded to a change in the equivalent angle of attack of approximately $\Delta\alpha = 0.7°$, which was equivalent to a 2° deflection of a plane flap having a C_f/c = 0.10. The real potential of this approach is in using multiple plasma actuators at different x/c locations. The effect of each of these actuators strongly depends on their chord locations and weakly depends on angle of attack. However their effect adds linearly so that for the conditions

used in the experiments reported here would produce the equivalent of 5.5° flap deflection of a trailing-edge flap, or approximately 2.75 times larger than with the single actuator.

The use of multiple actuators distributed at different chord location on the airfoil beautifully lends itself to digital control that would produce discrete changes in lift in response to dynamically changing rotor wind conditions. This is the basis for the Plasma Aerodynamic Control Effectors (PACE) system for improving wind turbine performance and control.

5. Plasma-Induced Flow Separation Control on a 3-D S827 Model

Wind tunnel experiments were conducted on a 3-D S827 model to examine the effects of a plasma actuator on controlling three-dimensional flow separations. The 3-D S827 model was used. A photograph of the 3-D S827 model is shown in **Figure 16**. Tests were conducted at a predetermined Re_c. Plasma actuators as described in Figure 8 were used to control leading-edge flow separation. Tufts were used to visualize/capture the effects of plasma on flow separation. A representative result from this study is shown in **Figure 17**.

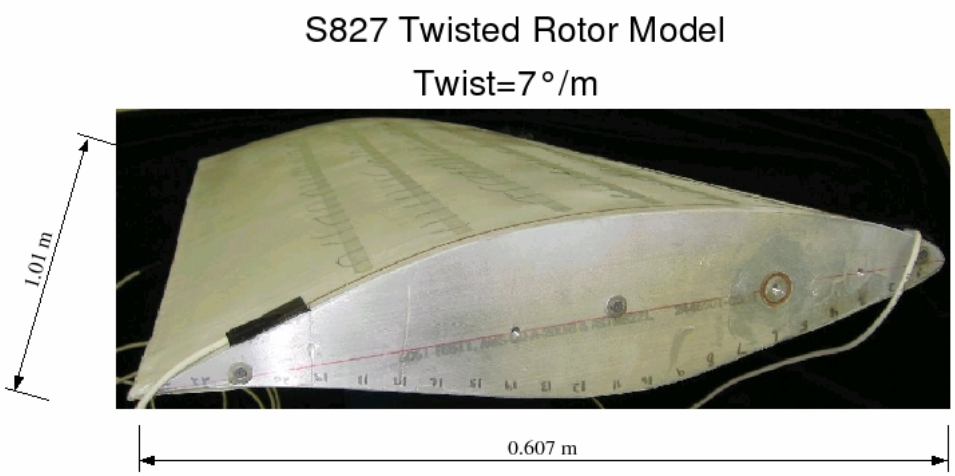

FIGURE 16: 3-D S827 blade model with 7°/m spanwise twist.

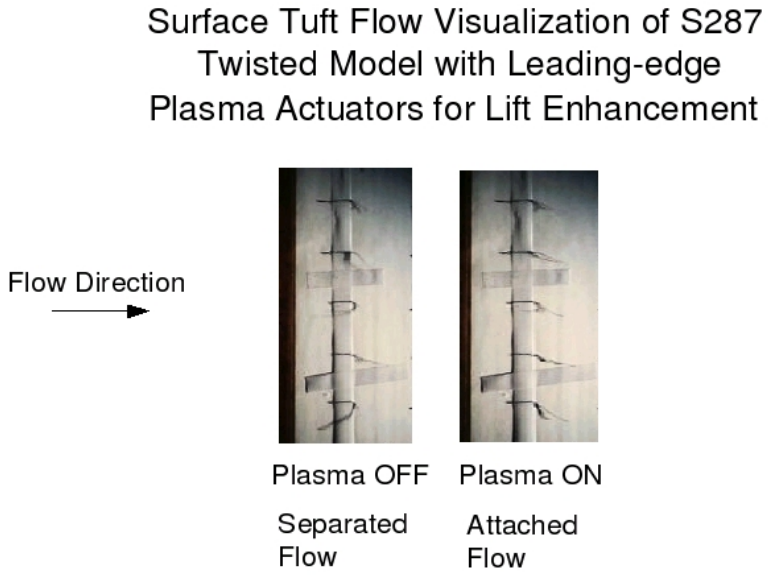

FIGURE 17: A photograph from an experiment conducted on the 3-D S827 blade model showing control of 3-D flow separation using a streamwise vortex generating leading-edge plasma actuator.

6. CFD Simulations of a Plasma Actuator on a 2-D S827 Model

The effect of the plasma actuator is incorporated into numerical flow solvers by adding the actuator body force into the momentum equation. Numerically, this is a particularly efficient approach because the body is not coupled to the flow parameters and therefore can be calculated off line for the particular geometry. This was performed for the S827 section shape using Fluent CFD software. Fluent uses a segregated solver to solve the 2-D Reynolds-averaged Navier-Stokes equations with a user defined input for adding the body Surface Tuft Flow Visualization of S287

Twisted Model with Leading-edge Plasma Actuators for Lift Enhancement force distribution to account for the plasma actuator effect. The computation was performed on a body-centered unstructured grid produced by GAMBIT.

The conditions for the simulation were identical to those used in the experiment and presented in Figure 7. For this study, the plasma actuator was the asymmetric design illustrated in Figure 1. Figure 18 shows the result of the simulation. Plotted is the lift coefficient at different angles of attack minus the lift coefficient at zero angle of attack. The solid curve is the base line condition. This shows the expected lift coefficient versus angle of attack slope in the linear range of 0.111/°. The effect of the actuator is identical to increasing the positive camber of the section shape, which is also equivalent to a positive deflection of a plane trailing-edge flap. This corresponds to a shift in the zero-lift angle of attack which amounts to a constant shift in the lift coefficient at all angles of attack in the linear range.

The change in lift in this simulation was approximately 0.024, about one-third of what was achieved in the experiment. We expect the CFD results to match with the wind tunnel data once the body force used in the CFD is fully matched with the experiment. Our aim in the simulation was to demonstrate that the effect of the actuator was identical to adding camber.

7. Gust Analysis to Estimate PACE Requirements to Maintain Control

To quantify the impact required by plasma actuators, particularly in the case of alleviating gust loading, a numerical analysis was conducted for an actual wind turbine generator before experimental testing. The wind turbine analyzed was a constant-speed, 17 m diameter generator examined in a case study in the Wind Energy Handbook [34]. If each blade is divided up into 10 sections, the largest aerodynamic and structural forces act on the three outermost sections. As a result, this analytical investigation was limited to these three sections. All required geometric and aerodynamic constants were drawn from the tables and figures listed in the case study.

With the geometry and aerodynamics constrained, values had to be chosen for three variables: the average wind velocity the tip speed ratio (A), and the gust factor (GF).

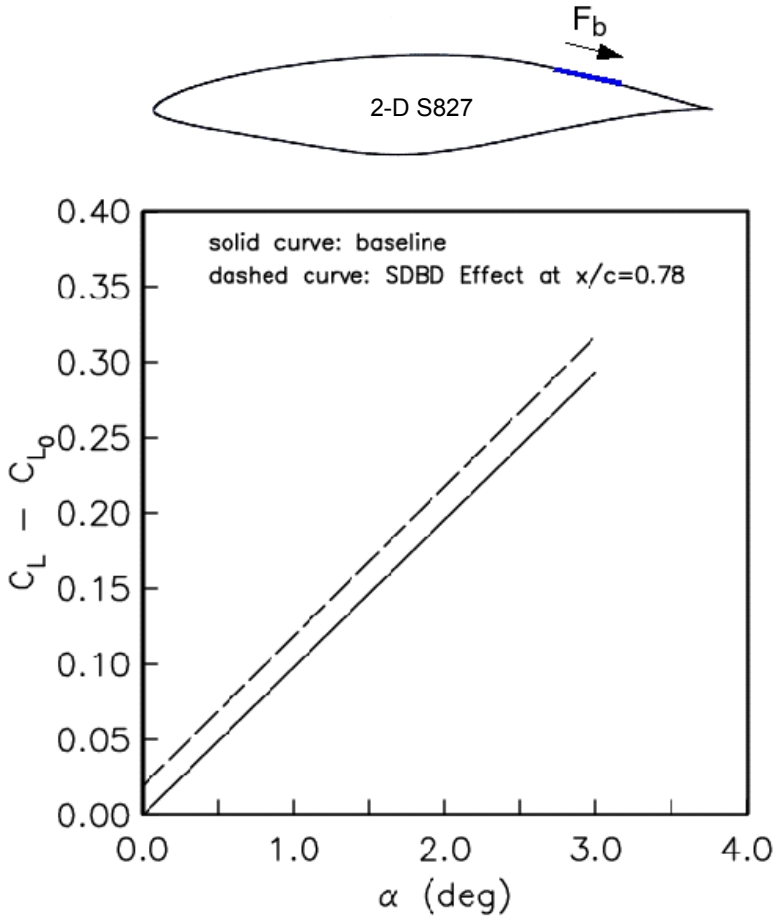

FIGURE 18: CFD modeling results showing lift control on a 2-D S827 model using a plasma actuator near the trailing-edge.

For this investigation, a wind velocity of 10 m/s was chosen. This fell between the turbine's cut-in speed of 4.5 m/s and wind speed for maximum power generation of 13 m/s. Four different tip speed ratios were analyzed: 3, 6, 9, and 12, with the optimal tip speed ratio for this turbine being 6. Lastly, gust factors, defined as the ratio of the gust velocity to the mean wind velocity, of 1.1, 1.3, 1.5, and 1.7 were investigated. The maximum gust factor of 1.7 was chosen because it was the largest examined in the Wind Energy Handbook [34].

The differential lift based upon simple blade element theory is given by [34]:

$$dL = \frac{1}{2}\rho C_L \left(U_\infty^2 + (r\omega)^2\right) c\,dr \tag{3}$$

For this analysis, a gust was assumed to directly add or subtract velocity from the average wind speed without changing its direction. Gusts influence two of the parameters above: the coefficient of lift, C_L, indirectly and the freestream velocity, U_∞, directly. Gusts do influence the coefficient of lift as gusts change the effective angle of attack. However, for this initial study, the effects due to the change in freestream velocity were assumed to have a greater influence, particularly for larger wind turbines that are set at lower angles of attack. Thus, only the influence on the U_∞ term due to the change in freestream velocity was included in this analysis. Lastly, corrections factors such as tip-loss factors or induction factors were not included because only the required change in coefficient of lift was desired. Since both the baseline lift and lift during gust were uncorrected, the change should remain approximately the same. Though approximate, these estimates should reflect the relative amount of change in coefficient of lift that would be needed to overcome the change in lift due to gust and will act as a simple guide.

For a constant speed turbine, with air density and the area of the blade element fixed, any change in average wind speed must be offset by a change in the coefficient of lift. Thus, to maintain constant lift, the coefficient of lift must change with the addition of gust loading. Normally, this would be achieved by some mechanical means of active flow control such as flaps or pitch to change the coefficient of lift. However, in this case, the plasma actuators would have to be able to provide this amount of change in lift slope. The required change in coefficient of lift in order to maintain constant lift is plotted in **Figure 19** for the optimal tip speed ratio of 6 and the 70 % to 80 % section (the blade section with the largest acting aerodynamic forces). As expected, the required change in lift steadily increases as wind speed, or in this case gust factor, increases. The maximum positive and negative changes required for this configuration was estimated to be 0.06 and -0.1 respectively.

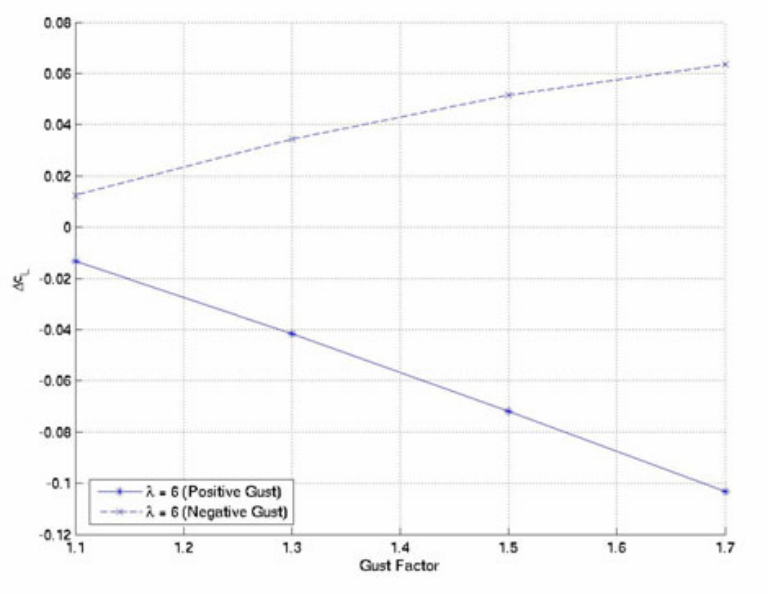

FIGURE 19: Required change in the 70% to 80% section for the optimal tip speed of 6.

Now, the results of the varying tip speed ratios and blades sections were examined (**Figures 20, 21, 22**). For any point in time, the wind turbine is ideally operating at a single tip speed ratio and is such on one color. After choosing the tip speed ratio, the gust factor and its direction can be selected and the corresponding necessary change in coefficient of lift can be estimated. Two immediate observations could be drawn from the analytical examination.

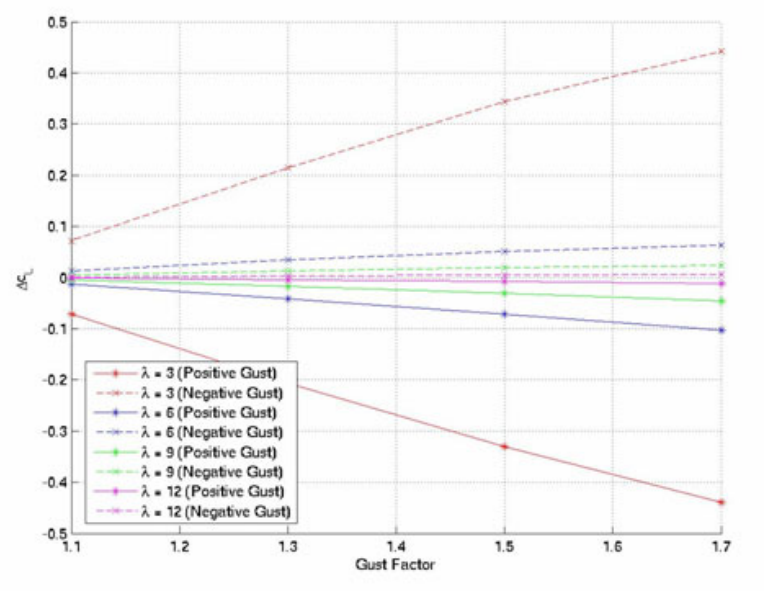

FIGURE 20: Required change in the 70% to 80% section for all tip speed ratios.

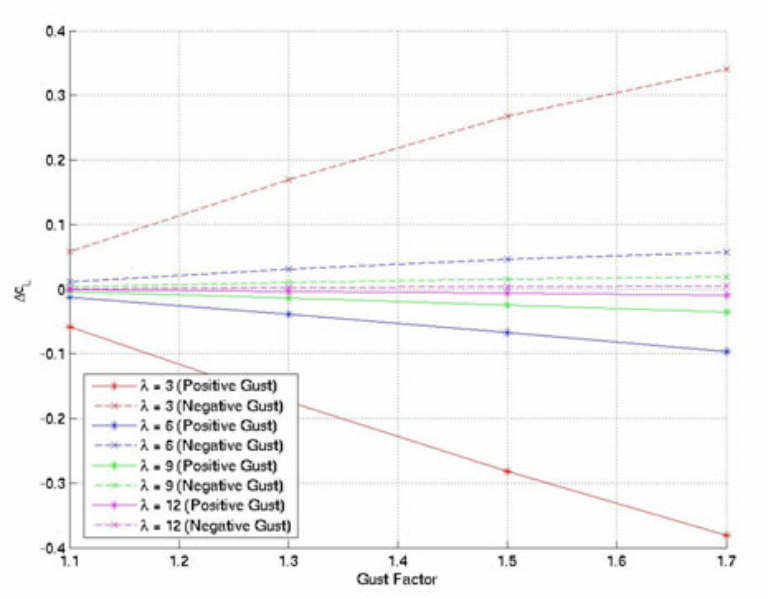

FIGURE 21: Required change in the 80% to 90% section for all tip speed ratios.

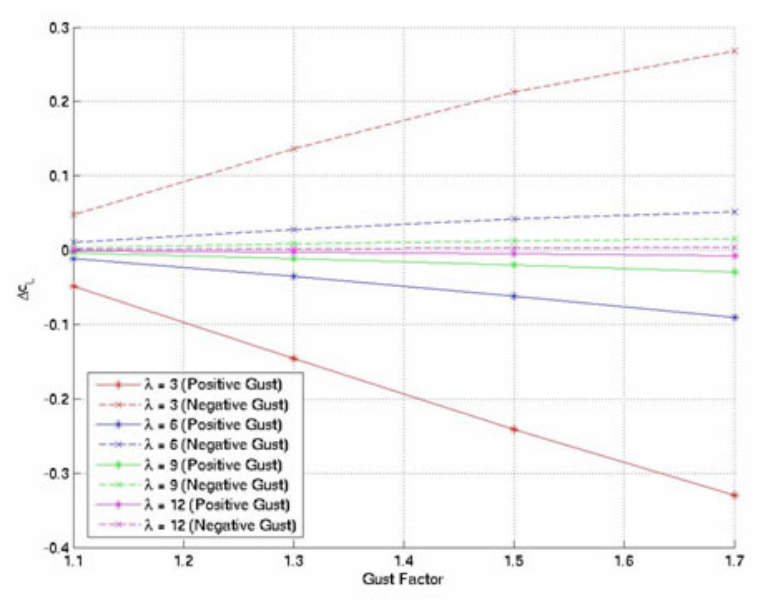

FIGURE 22: Required change in the 90% to 100% section for all tip speed ratios.

First, as tip speed ratios increase, the impact of gusts is minimized. For a very small tip speed ratio such as 3, however, a very large change in coefficient of lift would be required to offset the gust loading. This was expected because the differential lift on the blade element was proportional to the squares of the wind and rotational velocities. Thus, at very high rotational speeds, this term dominates and less required change was needed in the coefficient of lift. Another noticeable trend was the asymmetry between the positive and negative gusts. For every

gust factor, slightly less change in coefficient of lift was required for a negative gust as compared to a positive gust of the same magnitude. This was also due to the velocity terms being squared, because for a positive gust, the wind velocity component comprises a larger percentage of the relative speed.

Later, the effect of the gusts on effective angle of attack was incorporated into the analytical model. The same three blade sections were tested for positive gust factors ranging from 1.1 to 1.7. **Figure 23** depicts the estimates of the amount of change plasma actuators would have to create in order to maintain constant lift. Compared to the previous study, the maximum positive change required was approximately double that of the previous study. In this case, the maximum value was 0.21 respectively, compared to the earlier estimate of 0.10. However, the two studies produced different qualitative results as this new model now contains effects due to stall. In all cases, the smaller gusts all act to increase both the angle of attack and wind speed causing increased lift. This required a negative change in coefficient of lift to maintain constant lift. However, as gusts strengthen and continue to push the effective angle of attack higher, the blades begin to stall and begin producing less then optimal lift (despite the fact that the wind speed is greater than normal). As a result, the actuators actually have to increase the coefficient of lift. As sections go out toward the tip, the baseline angle of attack decreases. Thus, the 70% to 80% stalls first and requires the switch to a positive change in coefficient of lift first. The final section, 90% to 100%, never produces less than optimal lift for these gust factors though it

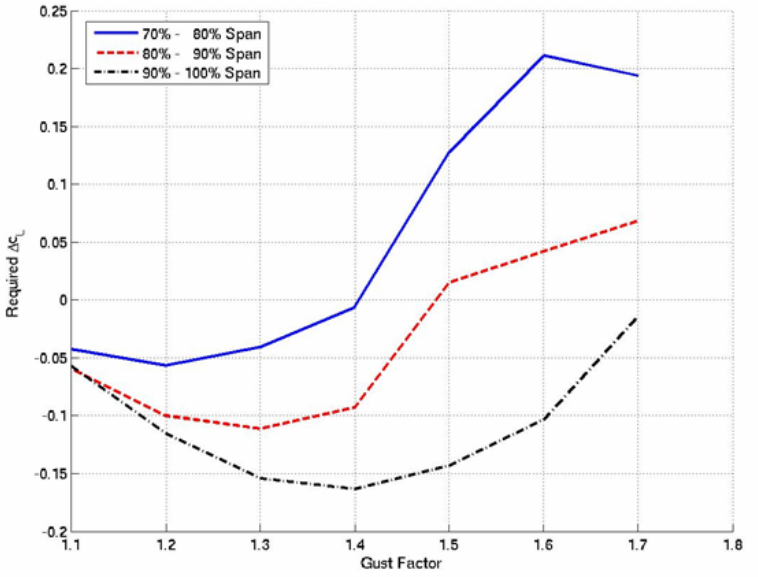

FIGURE 23: Required □CL to maintain constant lift under gust.

approaches stall. The quantitative results for the required change in coefficient of lift were determined along with the change in angle of attack due to gust. **Figures 24 and 25** depict the effective angles of attack in gust and the changes in angle of attack respectively.

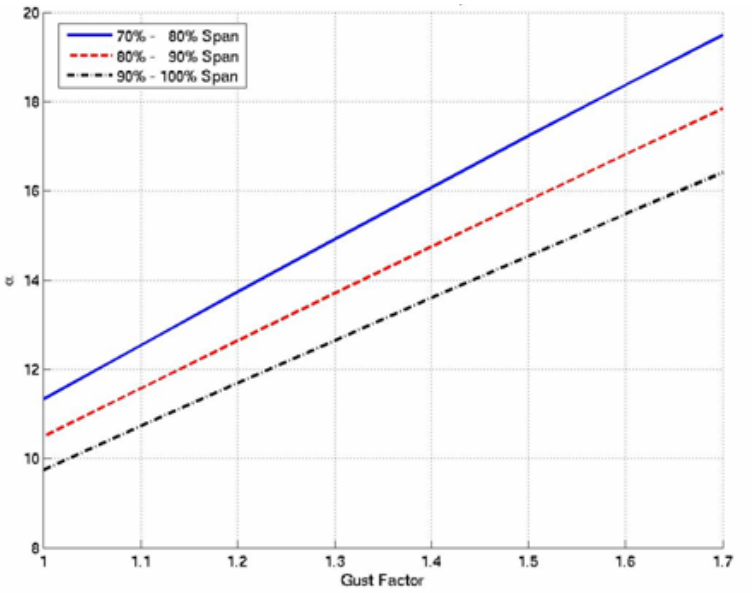

FIGURE 24: Influence of gust on effective angle of attack.

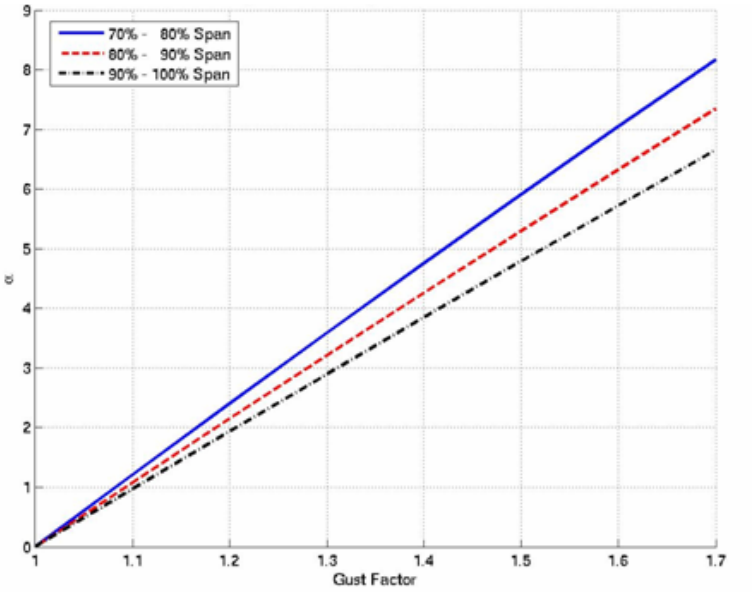

FIGURE 25: Change in effective angle of attack due to gust.

8. Effect of Rain and Sand on a Plasma Actuator

Preliminary experiments were conducted in a laboratory to examine the effects of water (simulated rain) and sand (simulated dust) on the operation of a plasma actuator. For the water experiment, a spray bottle was used to soak a section of the actuator. A dry actuator is shown in **Figure 26 (a)**. When the plasma actuator is completely soaked with water, it shuts off temporarily, only at the location where the water is present (see **Figure 26 (b)**), however, within seconds as most of the water is either evaporated or pushed away by the plasma, the actuator resumes its normal operation, with no change in its amplitude or frequency settings. This test was followed by a fatigue test where a portion of the plasma actuator was soaked with water repeatedly for over 30 minutes to simulate a rainy environment. This 30-minute fatigue test included ~25 cycles of plasma on/off under water conditions. After the end of the last cycle, a comparison was made between the time taken by the plasma actuator to recover in the last cycle versus the first cycle. No noticeable difference was found. This is an indication that water does not reduce the life-cycle or operating performance of a plasma actuator. With regard to the sand experiment, there were no negative effects whatsoever. Even after completely burying the actuator in sand, (see Figure 26 (c)) it continued to function normally. The plasma abruptly

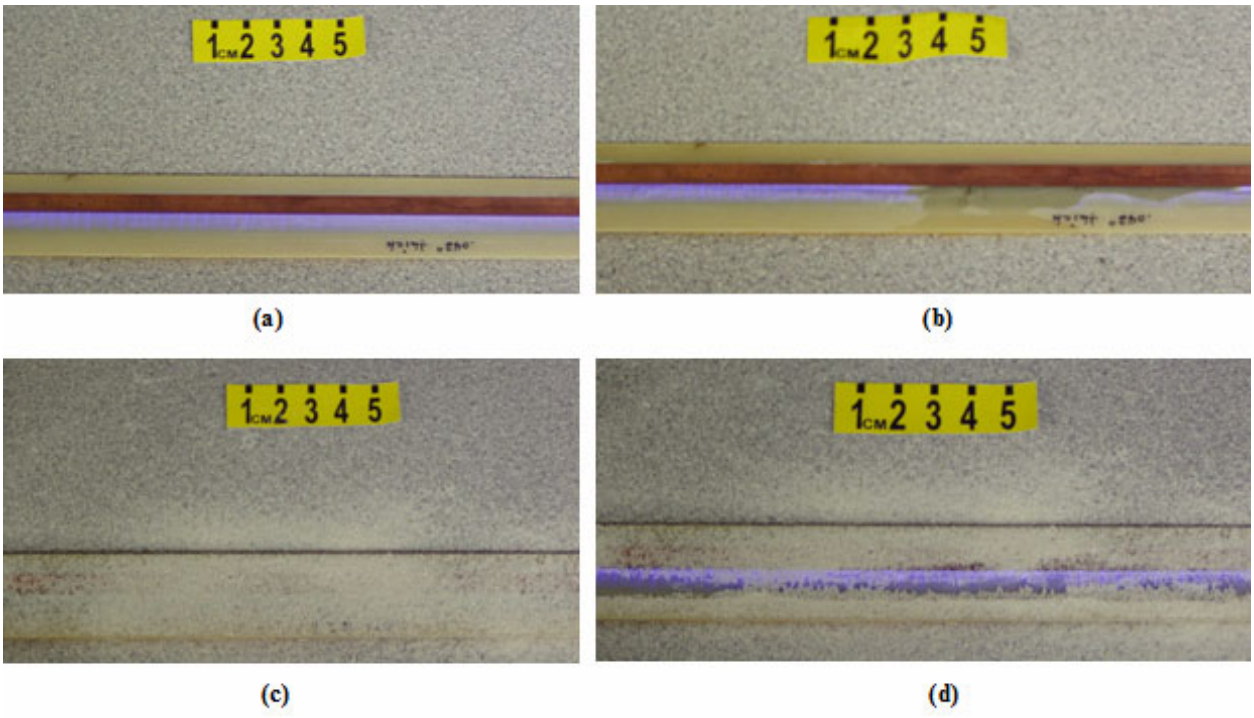

FIGURE 26: Results from the experiments conducted to study the effects of water and sand on the plasma actuator operation.

pushed the sand away from the actuator (see Figure 26 (d)), indicating that the actuator is not affected by the presence of dust or sand.

9. Power Considerations for a Plasma Actuator

The power required to operate the PACE system on a wind turbine is expected to be a small fraction of the power produced by the wind turbine itself. For example, a 50 m diameter 3-bladed wind turbine can typically generate over 700 kW of power with a 10 m/s wind speed, while requiring only 2550 W to operate the plasma actuators. This is less than 0.4% of the total power developed by the wind turbine.

Furthermore, an unsteady plasma actuator requires only 13 W per linear meter of turbine blade. A typical electronics package is approximately 75% efficient, yielding a total power requirement of 17 W per linear meter of turbine blade. Three 50 m blades equals 150 linear meters of blade and at 17 W per meter will require 2550 W of power. Even if multiple rows of plasma actuators are used on the blade, we do not anticipate all actuators to be operating in a simultaneous fashion.

To solve for the power developed by a 50 m diameter 3-bladed wind turbine, the following equation applies: $P = \left(\frac{1}{2}\right)\rho A U_{\infty}^{3}$) x cP where, P = power in watts, A = blade area in m², U_{∞} = wind velocity in m/s, p = the density of air (1.225 kg/m3), cP = the coefficient of power or Betz coefficient - the theoretical maximum efficiency (0.59), defined as the ratio of energy recovered to maximum recoverable energy which represents about 60% of the kinetic energy of the wind.

Figure 27 shows a wind turbine with one plasma actuator and associated electronics installed in each blade. The electronics can be imbedded near the tip of the blade where the mechanical stress on the blade is the lowest.

The power supply used by the Orbital Research plasma electronics is ±24 volts d.c. Virtually any power source can be converted to ±24 volts d.c. using low cost COTS power converters. This holds true whether the power source is alternating (a.c.) or direct current (d.c.). A wind turbine larger than a few kilowatts will need an alternate power source to electronically control yaw, pitch, rotor brakes, etc. This alternate power source will also be available for the plasma electronics. It is likely that a typical wind turbine will be connected to the existing power grid which will serve as an alternate power source. In either case, power will always be available to the plasma electronics regardless of wind speed.

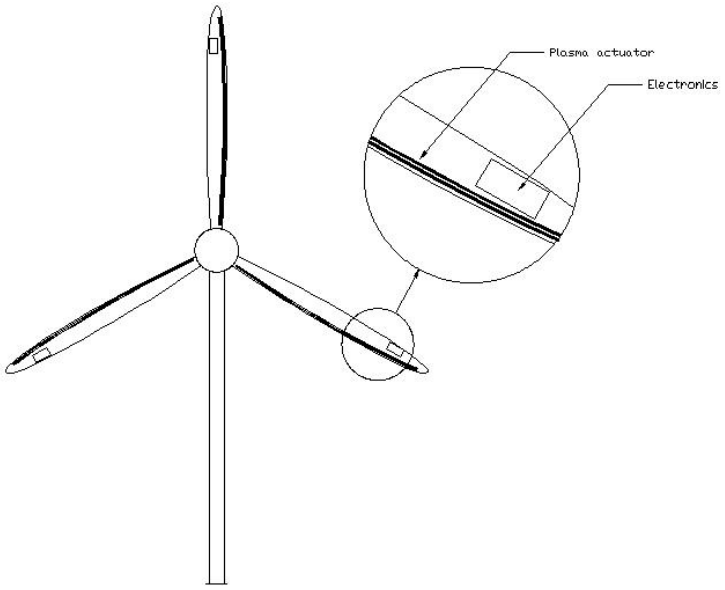

FIGURE 27: Example of a 3-blade wind turbine with one plasma actuator and associated electronics in each blade.

10. Dielectric Material Considerations for a Plasma Actuator

The insulator portion of a plasma actuator can be manufactured from a variety of materials. The most effective and durable material that we have found is Teflon film. A less expensive alternative is Kapton film which is commonly used as a substrate for flexible printed circuit boards. This type of actuator can be applied to the outside surface of the blade and look similar to shipping tape with adhesive on one side. This adhesive type actuator will make field replacement possible. Orbital Research had an actuator shown in **Figure 28** quoted by two different manufactures. For a quantity of 20 pieces, the cost is approximately $133 each. If this type of actuator is produced in large quantities, the cost is likely to be as low as a few dollars per meter.

This type of actuator is versatile in that it can be mounted on any surface. It is self contained and functional as a stand alone unit. Both electrodes required to develop plasma are imbedded within the insulating material.

The choice of the material used to insulate the two electrodes of a plasma actuator determines its useful life. Several candidate materials were tested for their ability to withstand heat and ozone; the two destructive components produced by plasma. The test criteria were to increase the voltage of each material to the point of failure. All of the materials tested failed

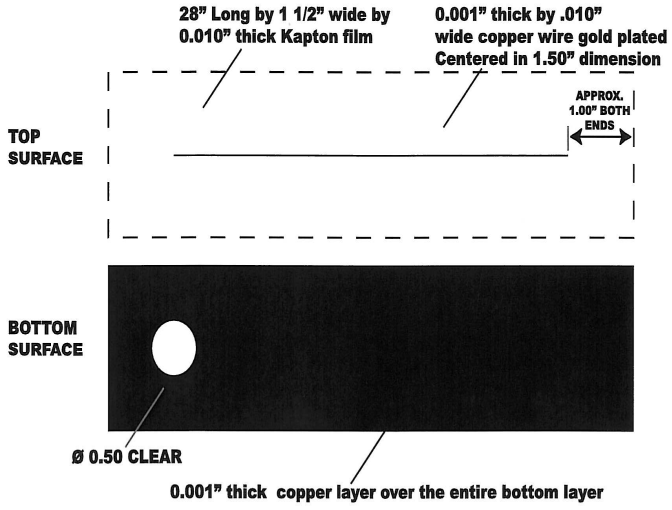

FIGURE 28: Flexible printed circuit of a plasma actuator.

instantly at the voltage shown below with the exception of the plate glass and fiberglass. The frequency of each actuator was adjusted to provide the best visible plasma. This frequency varies from one actuator to another as a function of actuator length, insulator type, insulator thickness, electrode spacing, and electrode width. The Kapton™ material used is a DuPont® product. A typical power level for a low speed airfoil is 20 watts per linear foot of actuator. All of the plasma photos shown above were tested at approximately 20 watts per linear foot with the exception of the plate glass, Teflon®, and fiberglass. A total of eight different materials were tested.

11. Conclusions

Single dielectric plasma actuators were demonstrated in experiments to provide lift control on two wind turbine blade section shapes designated S827 and S822. For the S822 section shape, the objective was to modify the baseline section shape to produce flow separation ramps that could be manipulated by the plasma actuators to produce different pressure distributions near the trailing edge, and thereby control the overall lift. The ramp sections were linear cuts having angles of 15° with respect to a line tangent to the surface at the airfoil maximum thickness point. The overall length of the airfoil would remain the same as the baseline.

Without separation control at the ramps, the lift distribution with angle of attack of the modified S822 airfoil fell below the baseline values. The maximum deviations occurring at approximately $\alpha = 3°$ and 11°. The deviation at the smaller angles of attack were due to the flow separation over the ramps. At the higher angles of attack, the deviations were due to a premature leading edge separation. The plasma actuator could recover the lost lift at the lower angles of attack between $-3° < \alpha < 3°$. In this range, the maximum change in lift between having the plasma actuator on and off was approximately $\Delta C_l = 0.4$. This is equivalent to a 10° deflection of a plane trailing-edge flap with a $C_f/C = 0.1$. This was performed with a periodically pulsed plasma actuator which reduced the power to the actuator by 90% over steady operation used for lift control based on circulation control.

For the S827 section shape, the objective was to use steady plasma actuators for circulation control that has been shown to be equivalent to increasing the effective camber of 2-D airfoil sections. The actuator resulted in a positive shift in the lift coefficient of approximately $\Delta C_l = 0.08$. This corresponded to a change in the equivalent angle of attack of approximately Aa = 0.7°, which was equivalent to a 2° deflection of a plane flap having a $C_f/C = 0.10$. The real potential of this approach is in using multiple plasma actuators at different x/c locations. The effect of each of these actuators strongly depends on their chord locations and weakly depends on angle of attack. However their effect adds linearly so that for the conditions used in the experiments reported here, three actuators at various locations would produce the equivalent of 5.5° flap deflection of a trailing-edge flap with $C_f/C = 0.1$, or approximately 2.75 times larger than with the single actuator a less optimal location.

The use of multiple actuators distributed at different chord location on the airfoil beautifully lends itself to digital control that would produce discrete changes in lift in response to

dynamically changing rotor wind conditions. This is the basis for the Plasma Aerodynamic Control Effectors (PACE) system for improving wind turbine performance and control.

References

[1] American Wind Energy Association, Global Wind Energy Market Report, 2001.

[2] Tangler, J. L. and Somers, D. M., NREL Airfoil Families for HAWTs, AWEA 95, March, 1995.

[3] Post, M. and T. Corke. 2003. Separation control on high angle of attack airfoil using plasma actuators. AIAA Paper 2003-1024, also 2006, AIAA J., 42, 11, p. 2177.

[4] Huang, J., Corke, T. and Thomas, F. 2003. Plasma actuators for separation control of low pressure turbine blades. AIAA Paper 2003-1027. AIAA J., 44, 1, pp. 51-58.

[5] Huang, J., Corke, T. and Thomas, F. 2006. Unsteady plasma actuators for separation control of low pressure turbine blades. AIAA J., 44, 7, pp. 1477-1487.

[6] Post, M. 2004. Plasma actuators for separation control on stationary and oscillating wings. Ph.D Dissertation, University of Notre Dame.

[7] Post, M. and Corke, T. 2004. Separation control using plasma actuators – stationary and oscillating airfoils. AIAA Paper 2004-0841.

[8] Corke, T., He, C. and Patel, M., 2004. Plasma flaps and slats: an application of weakly-ionized plasma actuators. AIAA Paper 2004-2127.

[9] Corke, T., E. Jumper, M. Post, D. Orlov, and T. McLaughlin. 2002. Application of weakly-ionized plasmas as wing flow-control devices. AIAA Paper 2002-0350.

[10] Corke, T., Mertz, B. and Patel, M. 2006. Plasma flow control optimized airfoil. AIAA Paper 2006-1208.

[11] Lopera, J., Ng, T. T., Patel, M. P., Vasudevan, S., Santavicca, E., and Corke, T. C., "Aerodynamic Control Using Windward-Surface Plasma Actuators on a Separation Ramp," J. of Aircraft, Vol. 44, No. 6, Nov-Dec 2007.

[12] Patel, M. P., Ng, T. T., Vasudevan, S., Corke, T. C., Post, M., McLaughlin, T. E., and Suchomel, C., "Scaling Effects of an Aerodynamic Plasma Actuator," J. of Aircraft, Vol. 45, No. 1, Jan-Feb 2008.

[13] Patel, M. P., Ng, T. T., Vasudevan, S., Corke, T. C., and He, C., "Plasma Actuators for Hingeless Aerodynamic Control of an Unmanned Air Vehicle," J. of Aircraft, Vol. 44, No. 4, pp. 1264-1274, July-Aug 2007. Also AIAA Paper 2006-3495.

[14] Patel, M. P., Sowle, Z. H., Corke, T. C., and He, C., "Autonomous Sensing and Control of Wing Stall Using a Smart Plasma Slat," J. of Aircraft, Vol. 44, No. 2, pp. 516527, March-April 2007. Also AIAA Paper 2006-1207.

[15] Enloe, L, T. McLaughlin, VanDyken, Kachner, E. Jumper, and T. Corke. 2004. Mechanisms and Response of a single dielectric barrier plasma actuator: Plasma morphology. AIAA J., 42, 3, p. 589. Also AIAA 2003-1021.

[16] Enloe, L, T. McLaughlin, VanDyken, Kachner, E. Jumper, T. Corke.. M. Post, O. Haddad. 2004. Mechanisms and Response of a single dielectric barrier plasma actuator: Geometric efects. AIAA J., 42, 3, p 585.

[17] Corke, T., Post, M. and Orlov, D. 2007. SDBD plasma enhanced aerodynamics: concepts, optimization and applications, Prog. Aerospace Sci., doi:10.1016/j.paerosci.2007.06.001, Elsevier Ltd.

[18] Orlov, D. and Corke, T. C., Numerical simulation of aerodynamic plasma actuator effects, AIAA Paper 2005-1083.

[19] Orlov, D., Corke, T., and Patel, M. 2006. Electric circuit model for aerodynamic plasma actuator. AIAA-2006-1206.

[20] Orlov, D. Modeling and simulation of single dielectric barrier discharge plasma actuators. Ph.D. University of Notre Dame, 2006.

[21] Miller, L. S., Quandt, G. A., Huang, S., Atmospheric Tests of Trailing-Edge Aerodynamic Devices, NREL SR -500-22350, 1998.

[22] Stuart, J. G., Wright, A. D. and Butterfield, C. P., Considerations for an Integrated Wind Turbine Controls Capability at the National Wind Technology Center: An AileronControl Case Study for Power Regulation and Load Mitigation, NREL - TP-440-21335, June 1996.

[23] Van Kuik, G., Barlas, T., and van Bussel, G., Smart Rotor and Control Concepts. Von Karman Institute for Fluid Dynamics Lecture Series entitled wind Turbine Aerodynamics

A State-of-the-Art, March 19-23, 2007.

[24] Somers, D. M., Design and Experimental Results for the S827 Airfoil, NREL/SR500-36345, January 2005.

[25] Somers, D. M., The S822 and S823 Airfoils, NREL/SR-500-36342, January 2005.

[26] Corke, T., Mertz, B. and Patel, M. Plasma flow control optimized airfoil, AIAA Paper 2006-1208.

[27] Nelson, S., Cain, A., Patel, M., and Corke, T., A simplified strategy for optimizing flow-control-configured airfoils, AIAA Paper 2007-4274-FCC.

[28] Hall, K., Jumper, E., Corke, T. and McLaughlin, T. Potential flow model of a plasma actuator as a lift enhancement device. AIAA Paper 2005-0783.

[29] Hall, K. Potential flow model for plasma actuation as a lift enhancement device. M.S. Thesis, University of Notre Dame, 2004.

[30] Corke, T. C., "Design of Aircraft," Prentice-Hall Publishers, New York, 2002.

[31] He, C., Corke, T. and Patel, M. Numerical and experimental analysis of plasma flow control over a hump model. AIAA Paper 2007-0935.

[32] He, C. Plasma slats and flaps: an application of plasma actuators for hingeless aero-dynamic control. Ph.D. University of Notre Dame. 2008.

[33] Iqbal,M., Corke, T. and Thomas, F. Parametric optimization of single dielectric barrier discharge (SDBD) plasma actuators. Submitted AIAA J., 2007.

[34] Burton, T., et al. "Wind Energy Handbook." New York: John Wiley & Sons, Ltd. 2001.

[35] Ashwill, T., and Laird, D, "Concepts to Facilitate Very Large Blades," AIAA Paper 2007-817, 45th AIAA Aerospace Sciences Meeting, Reno, NV, January 8-11, 2007.

[36] Berg, D. E., and Zagas, J. R., "Aerodynamic and Aeroacoustic Properties of Flat-back Airfoils," AIAA Paper 2008-1455, 46th AIAA Aerospace Sciences Meeting, Reno NV, January 7-10, 2008.

[37] Thomas, F. O., Kozlov, A., Corke, T. C., "Plasma Actuators for Landing Gear Noise Control," AIAA Paper 2005-3010, Proceedings of the 11th AIAA/CEAS Aeroacoustics Conference, Monterey, CA.